15 Semiconductor Lasers—Theory and Applications

15.0 INTRODUCTION

The semiconductor laser invented in 1961 [1–3] is the first laser to make the transition from a research topic and specialized applications to the mass consumer market. It is, by economic standards and the degree of its applications, the most important of all lasers.

The main features that distinguish the semiconductor laser are

1. Small physical size (300 μm $\times$ 10 μm $\times$ 50 μm) that enables it to be incorporated easily into other instruments.
2. Its direct pumping by low-power electric current (15 mA at 2 volts is typical), which makes it possible to drive it with conventional transistor circuitry.
3. Its efficiency in converting electric power to light. Actual operating efficiencies exceed 50 percent.
4. The ability to modulate its output by direct modulation of the pumping current at rates exceeding 20 GHz. This is of major importance in high-data-rate optical communication systems.
5. The possibility of integrating it *monolithically* with electronic field effect transistors, microwave oscillators, bipolar transistors, and optical components in III–V semiconductors to form integrated optoelectronic circuits.
6. The semiconductor-based manufacturing technology, which lends itself to mass production.
7. The compatibility of its output beam dimensions with those of typical

silica-based optical fibers and the possibility of tailoring its output wavelength to the low-loss, low-dispersion region of such fibers.

From the pedagogic point of view, understanding how a modern semiconductor laser works requires, in addition to the basic theory of the interaction of radiation with electrons that was developed in Chapter 5, an understanding of dielectric waveguiding [4, 5] (Section 13.1) and elements of solid-state theory of semiconductors [6, 7]. The latter theory will be taken up in the next few sections.

15.1 SOME SEMICONDUCTOR PHYSICS BACKGROUND

In this section we will briefly develop some of the basic background material needed to understand semiconductor lasers. The student is urged to study the subject in more detail, using any of the numerous texts dealing with the wave mechanics of solids (Reference [6], for example).

The main difference between electrons in semiconductors and electrons in other laser media is that in semiconductors all the electrons occupy, thus share, the whole crystal volume, while in a conventional laser medium, ruby, for example, the Cr^{3+} electrons are localized to within 1 or 2 Å of their parent Cr^{3+} ion and electrons on a given ion, for the typical Cr doping levels used, do not communicate with those on other ions.

In a semiconductor, on the other hand, because of the spatial overlap of their wavefunctions, no two electrons in a crystal can be placed in the same quantum state, i.e., possess the same eigenfunction. This is the so-called *Pauli exclusion principle,* which is one of the more important axiomatic foundations of quantum mechanics. Each electron thus must possess a unique spatial wavefunction and an associated eigenenergy (the total energy associated with the state). If we plot a horizontal line, as in Figure 15-1, for each allowed electron energy (eigenenergy), we will discover that the energy levels cluster within bands that are separated by "energy gaps" ("forbidden" gaps). A schematic description of the energy level spectrum of electrons in a crystal is shown in Figure 15-1.

The manner in which the available energy states are occupied determines the conduction properties of the crystal. In an insulator the uppermost occupied band is filled up with electrons while the next highest band is completely empty. The gap between them is large enough, say, ~3 eV, so that thermal excitation across the gap is negligible. If we apply an electric field to such an idealized crystal, no current will flow, since the electronic motion in a filled band is completely balanced and for each electron moving with a velocity $\mathbf{v}$ there exists another one with $-\mathbf{v}$.

If the gap between the uppermost filled band—the valence band—and the next highest—the conduction band—is small, say, <2 eV, then thermal excitation causes partial transfer of electrons from the valence band to the

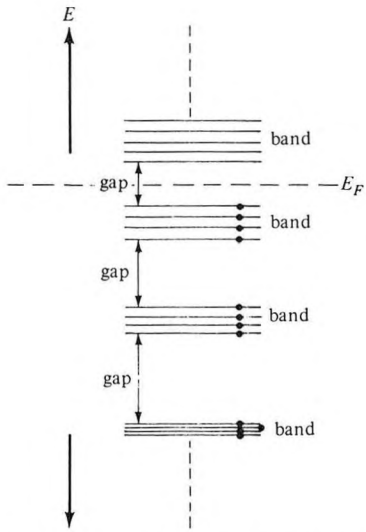

Figure 15-1 The energy levels of electrons in a crystal. In a given material these levels are usually occupied, in the ground state, up to some uppermost level. The energy E_F that marks in the limit of $T \to 0$, the transition from fully occupied electron states ($E < E_F$) to empty states ($E > E_F$), is called the *Fermi energy*. It does not, except accidentally, correspond to an eigenenergy of an electron in the crystal.

conduction band and the crystal can conduct electricity. Such crystals are called *semiconductors*. Their degree of conductivity can be controlled not only by the temperature but by "doping" them with impurity atoms.

The wavefunction of an electron in a given band, say, the valence, is characterized by a vector **k** and a corresponding (Bloch) wavefunction

$$\psi_v(\mathbf{r}) = u_{v_\mathbf{k}}(\mathbf{r})\, e^{i\mathbf{k}\cdot\mathbf{r}} \tag{15.1-1}$$

The function $u_{v_\mathbf{k}}$ possesses the same periodicity as the lattice. The factor $\exp(i\mathbf{k}\cdot\mathbf{r})$ is responsible for the wave nature of the electronic motion and is related to the de Broglie wavelength λ_e of the electron by[1]

$$\lambda_e = \frac{2\pi}{k} \tag{15.1-2}$$

The vector **k** can only possess a prescribed set of values (i.e., it is quantized), which is obtained by requiring that the total phase shift $\mathbf{k}\cdot\mathbf{r}$ across a crystal with dimensions L_x, L_y, L_z be some multiple integer of 2π.

$$k_i = \frac{2\pi}{L_i}\, s \qquad s = 1, 2, 3, \ldots \tag{15.1-3}$$

[1]This is true if the value of **k** is taken in the extended (i.e. not reduced) **k** space.

where $i = x, y, z$. We can thus divide the total volume in **k** space into cells each with a volume

$$\Delta V_k \equiv \Delta k_x \, \Delta k_y \, \Delta k_z = \frac{(2\pi)^3}{L_x L_y L_z} = \frac{(2\pi)^3}{V} \tag{15.1-4}$$

and associate with each such differential volume a quantum state (two states when we allow for the two intrinsic spin states of each electron). The number of such states within a spherical shell (in **k** space) of radial thickness dk and radius k is then given by the volume of the shell divided by the volume (15.1-4) ΔV_k per state

$$\rho(k)dk = \frac{k^2 V}{\pi^2} \, dk \tag{15.1-5}$$

so that $\rho(k)$ is the number of states per unit volume of **k** space. (A factor of 2 for spin was included.)

The energy, measured from the bottom of the band, of an electron **k** in, say, the conduction band (indicated henceforth by a subscript c) is

$$E_c(\mathbf{k}) = \frac{\hbar^2 k^2}{2m_c} \tag{15.1-6}$$

where m_c is the effective mass of an electron in the conduction band. In the simplest and idealized case, which is the one we are considering here, the energy depends only on the magnitude k of the electron propagation vector and not its direction.

We often need to perform electron counting, not in **k** space but as a function of the energy. The density of states function $\rho(E)$ (the number of electronic states per unit energy interval per unit crystal volume) is determined from the conservation of states relation

$$\rho(E) \, dE = \frac{1}{V} \rho(k) \, dk$$

which with the use of (15.1-5) and (15.1-6) leads to

$$\rho_c(E) = \frac{1}{2\pi^2} \left(\frac{2m_c}{\hbar^2} \right)^{3/2} E^{1/2}$$

or

$$\rho_c(\omega) = \hbar \rho_c(E) = \frac{1}{2\pi^2} \left(\frac{2m_c}{\hbar} \right)^{3/2} \omega^{1/2} \tag{15.1-7}$$

where $\hbar\omega = E$. A similar expression but with m_c replaced by m_v, the effective mass in the valence band, applies to the valence band.

Figure 15-2 depicts the energy$-k$ relationship of a direct gap semiconductor, i.e., one where the conduction band minimum and the valence band

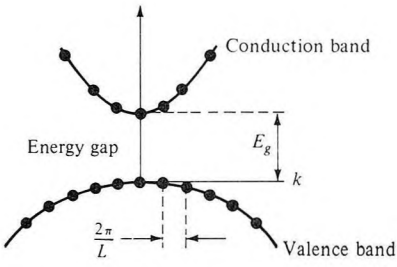

Figure 15-2 A typical energy band structure for a direct gap semiconductor with $m_c < m_v$. The uniformly spaced dots correspond to electron states.

maximum occur at the same value of **k**. The dots represent allowed (not necessarily occupied) electron energies. Note that, following (15.1-3), these states are spaced uniformly along the k axis.

The Fermi–Dirac Distribution Law

The probability that an electron state at energy E is occupied by an electron is given by the Fermi–Dirac law [6, 7]

$$f(E) = \frac{1}{e^{(E-E_F)/kT} + 1} \tag{15.1-8}$$

where E_F is the Fermi energy and T is the temperature. For electron energies well below the Fermi level such that $E_F - E \gg kT$, $f(E) \rightarrow 1$ and the electronic states are fully occupied, while well above the Fermi level $E - E_F \gg kT$, $f(E) \propto \exp(-E/kT)$ and approaches the Boltzmann distribution. At $T = 0$ $f(E) = 1$, for $E < E_F$, and $f(E) = 0$, for $E > E_F$ so that all levels below the Fermi level are occupied while those above it are empty. In thermal equilibrium a single Fermi energy applies to both the valence and conduction bands. Under conditions in which the thermal equilibrium is disturbed, such as in a p-n junction with a current flow or a bulk semiconductor in which a large population of conduction electrons and holes is created by photoexcitation, separate Fermi levels called *quasi-Fermi levels* are used for each of the bands. The concept of quasi-Fermi levels in excited systems is valid whenever the carrier scattering time within a band is much shorter than the equilibration time between bands. This is usually true at the large carrier densities used in p-n junction lasers.

In very highly doped semiconductors, the Fermi level is forced into either (1) the conduction band for donor impurity doping or (2) into the valence band for acceptor impurity doping. This situation is demonstrated by Figure 15-3. According to (15.1-8) at 0 K, all the states below E_F are filled while those above it are unoccupied as shown in the figure. In this respect the degenerate semiconductor behaves like a metal in which case the con-

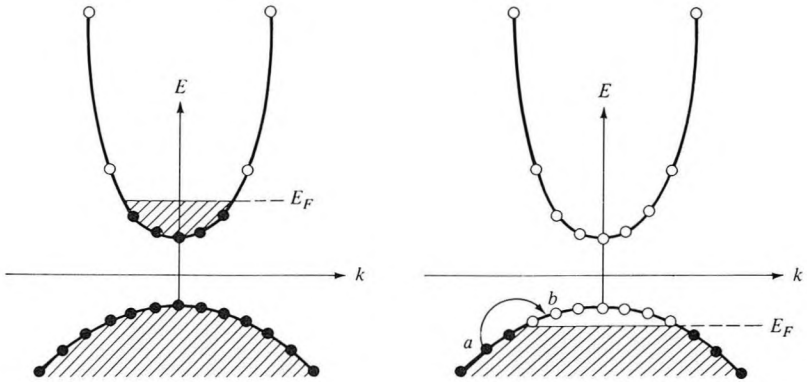

Figure 15-3 (a) Energy band of a degenerate n-type semiconductor at 0 K. (b) A degenerate p-type semiconductor at 0 K. The cross-hatching represents regions in which all the electron states are filled. Empty circles indicate unoccupied states (holes).

ductivity does not disappear at very low temperatures. The unoccupied states in the valence band [unshaded area in Figure 15-3(b)] are called *holes*, and they are treated exactly like electrons except that their charge, corresponding to an electron deficiency, is positive and their energy increases downward in the diagram. The number of holes in the semiconductor depicted by Figure 15-3(b) is the number of electron states falling within the unshaded area at the top of the valence band. The process of exciting an electron from state a to state b [Figure 15.3(b)] in the valence band can also be viewed as one whereby a hole is excited from b to a. The advantage of this point of view is the symmetry in the language and mathematical description that it brings to the discussions of current flow due to electrons in the conduction band and those in the valence band.

To better appreciate the role of the quasi-Fermi level, consider a non-thermal equilibrium situation in which electrons are excited into the conduction band of a degenerate p-type semiconductor at a very high rate. This can be done by injecting electrons into the p region across a p-n junction or by subjecting the semiconductor to an intense light beam with $h\nu > E_g$, so that for each absorbed photon an electron is excited into the conduction band from the valence band. This situation is depicted in Figure 15-4. Following this excitation, electrons relax, by emitting optical and acoustic phonons, to the bottom of the conduction band in times of $\sim 10^{-12}$ s while their relaxation across the gap back to the valence band—a process referred to as electron-hole recombination—is characterized by a time constant of

$$\tau \sim 3 - 4 \times 10^{-9} \text{ s}$$

It is important in analyzing the process of light amplification in semicon-

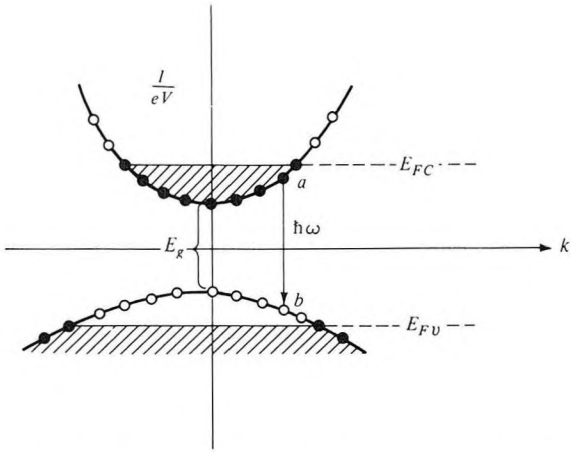

Figure 15-4 Electrons are injected at a rate of I/eV per unit volume (I = total current) into the conduction band of a semiconductor.

ductors to determine the quasi-Fermi level E_{F_c} for a given rate of excitation. Assuming that the relaxation to the bottom of the band into which the carriers are excited is instantaneous, we have

$$\frac{N_c}{\tau} = \frac{I}{\mathrm{eV}} \tag{15.1-9}$$

where N_c is the density (m^{-3}) of electrons in the conduction band, I the injection current (in amperes), τ is the electron relaxation time back to the valence band (electron-hole recombination time), and V is the volume into which the electrons are confined following injection. The density of electrons with energies between E and $E + dE$ is the product of $\rho_c(E)$—the density of allowed electron states—and the occupation probability $f_c(E)$ of these states.

Using (15.1-7) and (15.1-8),

$$\begin{aligned} N_c = \frac{I\tau}{\mathrm{eV}} &= \int_0^\infty \rho_c(E) f_c(E)\, dE \\ &= \frac{1}{2\pi^2}\left(\frac{2m_c}{\hbar^2}\right)^{3/2} \int_0^\infty \frac{E^{1/2}}{e^{(E-E_{F_c})/kT} + 1}\, dE \end{aligned} \tag{15.1-10}$$

For a given injection current I the only unknown quantity in (15.1-10) is the conduction quasi-Fermi level E_{F_c}. We can thus invert, in practice by numerical methods, (15.1-10) and solve it for $E_{F_c}(T)$ as a function of I, or equivalently of N_c. We shall make use, later, of this fact. At $T = 0$ the integral is replaced by

$$\int_0^{E_F} E^{1/2}\, dE = \tfrac{2}{3}E_F^{3/2}$$

yielding

$$E_F(T = 0) = (3\pi^2)^{2/3} \frac{\hbar^2}{2m_c} N_c^{2/3} \tag{15.1-11}$$

Another fact that we need before proceeding to the subject of optical gain in semiconductors is that when an electron makes a transition (induced or spontaneous) between a conduction band state and one in the valence band, the two states involved must have the same **k** vector. This is due to the fact that according to quantum mechanics the rate of such a transition is always proportional to an integral over the crystal volume that involves the product of the initial state wavefunction and the complex conjugate of that of the final state. Such an integral would, according to (15.1-1), be vanishingly small except when the condition

$$\mathbf{k}_f = \mathbf{k}_i \tag{15.1-12}$$

is satisfied. In band diagrams such as that of Figure 15-4, the transitions are consequently described by vertical arrows.

15.2 GAIN AND ABSORPTION IN SEMICONDUCTOR (laser) MEDIA

Consider the semiconductor material depicted in Figure 15-5 in which by virtue of electron pumping a nonthermal equilibrium steady state is obtained in which *simultaneously* large densities of electrons and holes coexist in the *same* space. These are characterized by quasi-Fermi levels E_{F_c} and E_{F_v}, respectively, as shown.

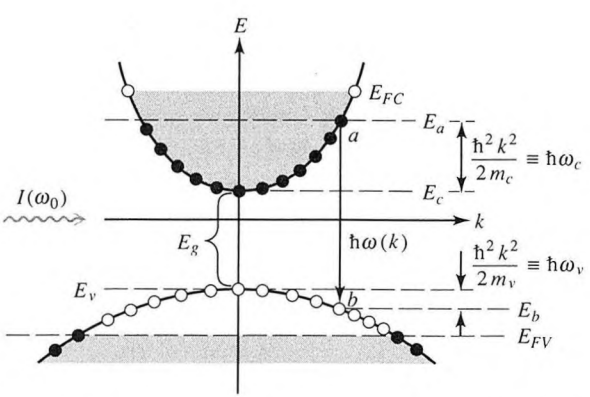

Figure 15-5 An optical beam at ω_0 with intensity $I(\omega_0)$ is incident on a pumped semiconductor medium characterized by quasi-Fermi levels E_{F_c} and E_{F_v}. A single level pair *a*-*b* with the same **k** value is shown. The induced transition $a \rightarrow b$ contributes one photon to the beam.

Let an optical beam at a (radian) frequency ω_0 travel through the crystal. This beam will induce downward $a \rightarrow b$ transitions that lead to amplification as well as $b \rightarrow a$ absorbing transitions. Net amplification of the beam results if the rate of $a \rightarrow b$ transitions exceeds that of $b \rightarrow a$.

As discussed in the previous section, only transitions in which the upper and lower electron states have the same **k** vector are allowed. The pair of levels a and b in Figure 15-5 are thus characterized by some **k** value. Let us consider a group of such levels with nearly the same **k** value and hence with nearly the same transition energy

$$\hbar\omega(\mathbf{k}) = E_g + \frac{\hbar^2 k^2}{2m_c} + \frac{\hbar^2 k^2}{2m_v} \tag{15.2-1}$$

(In the following the **k** dependence of ω will be omitted but understood.) The density of such level pairs whose **k** values fall within a spherical shell of thickness dk is, according to (15.1-5), $\rho(k)\, dk/V$.

Before proceeding let us remind ourselves of some results developed in connection with conventional laser media. The gain constant $\gamma(\omega_0)$ is given by (5.4-22) as

$$\gamma(\omega_0) = -\frac{k}{n^2}\chi''(\omega_0) \qquad k = \frac{2\pi n}{\lambda} \tag{15.2-2}$$

where $\chi''(\omega_0)$, the imaginary part of the electric susceptibility, is

$$\chi''(\omega_0) = \frac{(N_1 - N_2)\lambda_0^3}{8\pi^3 t_{\text{spont}}\, \Delta\nu n} \frac{1}{1 + 4(\nu - \nu_0)^2/(\Delta\nu)^2} \tag{15.2-3}$$

Combining the last two equations and defining the "relaxation time" T_2 by $T_2 = (\pi\, \Delta\nu)^{-1}$ leads to

$$\gamma(\omega_0) = \frac{(N_2 - N_1)\lambda_0^2}{4n^2 t_{\text{spont}}} \frac{T_2}{\pi[1 + (\omega - \omega_0)^2 T_2^2]} \tag{15.2-4}$$

In semiconductors T_2 is the mean lifetime for coherent interaction of k electrons with a monochromatic field and is of the order of the phonon-electron collision time. Numerically $T_2 \sim 10^{-12}$ s. Given an electron in an upper state "a," the lower state "b" with the same **k** value may be occupied by another electron. The downward rate of transitions is thus proportional to

$$R_{a\rightarrow b} \propto f_c(E_a)[1 - f_v(E_b)]$$

i.e., to the product of the probabilities $f_c(E_a)$ that the upper (conduction) state is occupied and the probability $(1 - f_v)$ that the lower (valence) state is empty. The functions $f_{v,c}(E)$ are given, according to (15.1-8), by

$$f_c(E) = \frac{1}{e^{(E - E_{F_c})/kT} + 1} \tag{15.2-5}$$

$$f_v(E) = \frac{1}{e^{(E-E_{F_v})/kT} + 1} \tag{15.2-6}$$

allowing for the fact that under pumping conditions $E_{F_c} \neq E_{F_v}$.

In translating to the case of semiconductors the results that were developed for conventional lasers, the population inversion density $(N_2 - N_1)$ is thus replaced by the effective inversion due to electrons and holes within dk.

$$N_2 - N_1 \rightarrow \frac{\rho(k)\,dk}{V}\{f_c(E_a)[1 - f_v(E_b)] - f_v(E_b)[1 - f_c(E_a)]\}$$

$$= \frac{\rho(k)\,dk}{V}[f_c(E_a) - f_v(E_b)] \tag{15.2-7}$$

$$E_a - E_b \equiv \hbar\omega = E_g + \frac{\hbar^2k^2}{2m_c} + \frac{\hbar^2k^2}{2m_v} \tag{15.2-8}$$

Equation (15.2-7) is of central importance and is a capsule statement of the difference between the population inversion in a conventional laser medium where the level occupation probability obeys Boltzmann statistics and that of a semiconductor medium governed by Fermi–Dirac statistics.

Returning to the gain expression (15.2-4), we use (15.2-7) to rewrite it as

$$d\gamma(\omega_0) = \frac{\rho(k)\,dk}{V}(f_c - f_v)\frac{\lambda_0^2}{4n^2\tau}\left(\frac{T_2}{\pi[1 + (\omega - \omega_0)^2T_2^2]}\right)$$

The differential designation $d\gamma(\omega_0)$ is to remind us that only electrons with $\mathbf{k}$ vectors within dk are included here. We have also replaced, to agree with popular usage, the term spontaneous lifetime (t_{spont}) by the recombination lifetime τ for an electron in the conduction band with a hole in the valence band. To obtain the gain constant, we must add up the contributions from all the electrons

$$\gamma(\omega_0) = \int_0^\infty \frac{dk\,\rho(k)}{V}[f_c(\omega) - f_v(\omega)]\frac{\lambda_0^2}{4n^2\tau}\left(\frac{T_2}{\pi[1 + (\omega - \omega_0)^2T_2^2]}\right) \tag{15.2-9}$$

We will find it easier to carry out the indicated integration in (15.2-9) in the ω domain [$\hbar\omega$ being the separation $E_a(\mathbf{k}) - E_b(\mathbf{k})$]. If we refer to Figure 15-5, we find that there exists a one-to-one correspondence

$$\hbar\omega = E_g + \frac{\hbar^2}{2m_r}k^2 \tag{15.2-10}$$

$$\frac{1}{m_r} = \frac{1}{m_v} + \frac{1}{m_c} \qquad (m_r \equiv \text{reduced effective mass}) \tag{15.2-11}$$

between ω and k. Using the relations

$$d\omega = \frac{\hbar}{m_r} k\, dk$$

$$\mathrm{k} = (\hbar\omega - E_g)^{1/2} \left(\frac{2m_r}{\hbar^2}\right)^{1/2}$$

the expression (15.2-9) for $\gamma(\omega_0)$ becomes

$$\gamma(\omega_0) = \int_0^\infty (\hbar\omega - E_g)^{1/2} \left(\frac{2m_r}{\hbar^2}\right)^{1/2} \frac{m_r \lambda_0^2 T_2 [f_c(\omega) - f_v(\omega)]}{\pi^2 \hbar 4n^2 \tau \pi [1 + (\omega - \omega_0)^2 T_2^2]} d\omega \qquad (15.2\text{-}12)$$

In most situations we can replace the normalized function

$$\frac{T_2}{\pi[1 + (\omega - \omega_0)^2 T_2^2]} \rightarrow \delta(\omega - \omega_0)$$

which is merely a statement of the fact that its width $\Delta\omega \sim T_2^{-1}$ is narrower than other spectral features of interest. In this case the integration (15.2-12) leads to

$$\gamma(\omega_0) = \frac{\lambda_0^2}{8\pi^2 n^2 \tau} \left(\frac{2m_c m_v}{\hbar(m_v + m_c)}\right)^{3/2} \left(\omega_0 - \frac{E_g}{\hbar}\right)^{1/2} [f_c(\omega_0) - f_v(\omega_0)] \qquad (15.2\text{-}13)$$

The condition for net gain $\gamma(\omega_0) > 0$ is thus

$$f_c(\omega_0) > f_v(\omega_0) \qquad (15.2\text{-}14)$$

which is the equivalent, in a semiconductor, of the conventional inversion condition $N_2 > N_1$. Using (15.2-5) and (15.2-6), the gain condition (15.2-14) becomes

$$\frac{1}{e^{(E_a - E_{F_c})/kT} + 1} > \frac{1}{e^{(E_b - E_{F_v})/kT} + 1} \qquad (15.2\text{-}15)$$

Recalling that $E_a - E_b = \hbar\omega_0$, (15.2-15) is satisfied provided

$$\hbar\omega_0 < E_{F_c} - E_{F_v} \qquad (15.2\text{-}16)$$

so that only frequencies whose photon energies $\hbar\omega_0$ are smaller than the quasi-Fermi levels separation are amplified. Condition (15.2-16) was first derived by Basov, et al. [1], Bernard and Duraffourg [8]. The general features of the gain dependence $\gamma(\omega_0)$ on the frequency ω_0 are illustrated by Figure 15-6. The gain is zero at $\hbar\omega < E_g$, since no electronic transitions exist at these energies. The gain becomes zero again at the frequency where $\hbar\omega_0 = E_{F_c} - E_{F_v}$. At higher frequencies the semiconductor absorbs.

Figure 15-7 shows calculated plots based on (15.2-12) with the density of the (injected) electrons as a parameter. The curves are based on the following physical constants of GaAs: $m_c = 0.067m_e$, $m_v = 0.48m_e$, $T_2 \sim 0.5$ ps, $\tau \simeq 3 \times 10^{-9}$ s, $E_g = 1.43$ eV. We note that the minimum density to

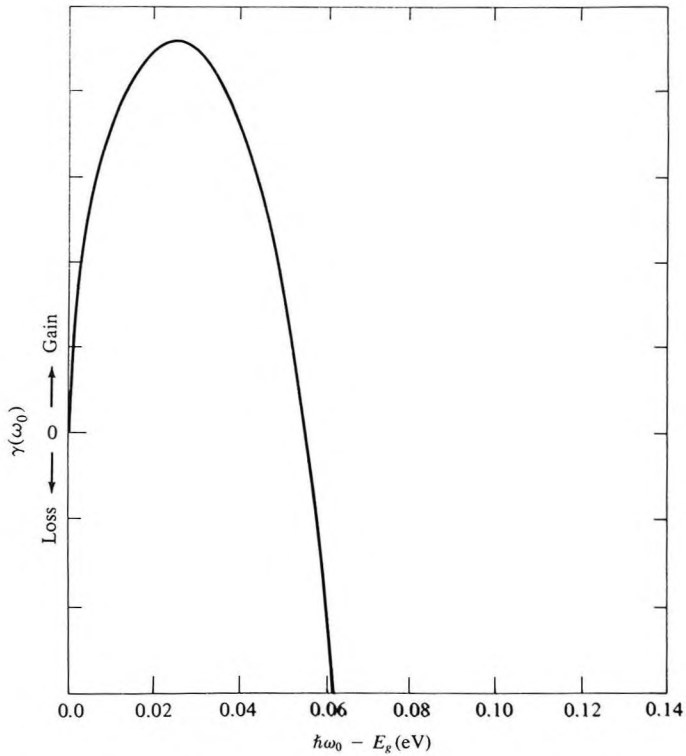

Figure 15-6 A typical plot of gain $\gamma(\omega_0)$ as a function of frequency for a fixed pumping level N. (After Reference [9].)

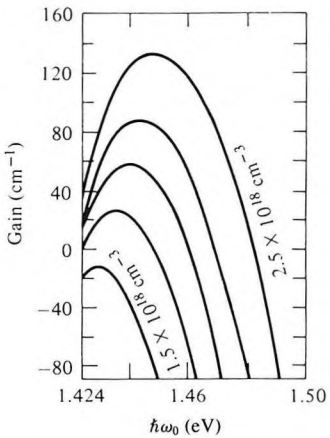

Figure 15-7 A plot based on (15.2-12) of the photon energy dependence of the optical gain (or loss = negative gain) of GaAs with the injected carrier density as a parameter. (After Reference [9].)

achieve transparency ($\gamma = 0$) is $N_{tr} \sim 1.55 \times 10^{18}$ cm^{-3}. The peak gain corresponding to a given inversion density N_c is plotted in Figure 15-8.

It follows from Figure 15-8 that semiconductor media are capable of achieving very large gain ranging up to a few hundred cm^{-1}. In a laser the amount of gain that actually prevails is clamped by the phenomenon of saturation (see Section 5.6) to a value equal to the loss. In a typical semiconductor laser this works out to $20 < \gamma < 80$ cm^{-1}. In this region we can approximate the plot of Figure 15-8 by a linear relationship

$$\gamma_{max} = B(N - N_{tr}) \tag{15.2-17}$$

The constant B fitting the data of Figure 15-8 is $B \sim 1.5 \times 10^{-16}$ cm^2 and is typical of GaAs/GaAlAs lasers at 300 K. The gain constant B increases with the decrease of the temperature T. This is due to the narrowing of the transition regions of the Fermi functions $f_c(\omega)$ and $f_v(\omega)$ in (15.2-12). At 77 K, $B \sim 5 \times 10^{-16}$ cm^2. Figure 15-8 shows that the semiconductor diode is capable of producing extremely large incremental gains, with only moderate

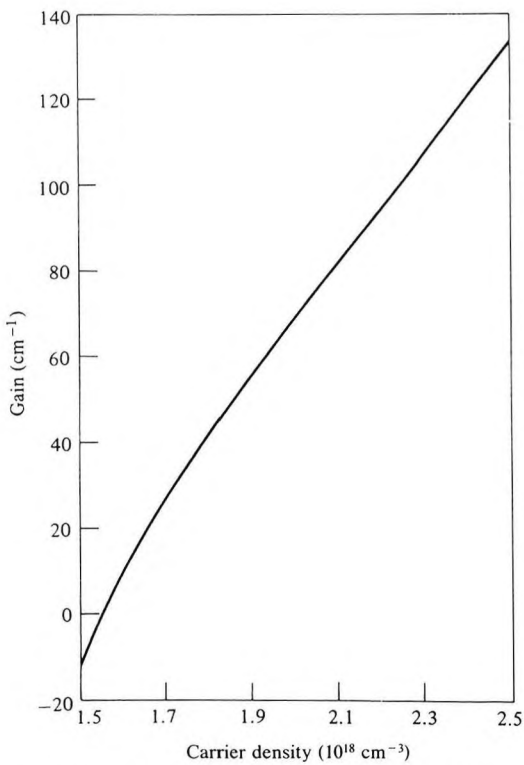

Figure 15-8 A plot of the peak gain γ_{max} of Figure 15-7 as a function of the inversion density at $T = 300$ K.

increases of the inversion density, hence the current, above the transparency value ($N_{tr} \sim 1.55 \times 10^{18}$ cm^{-3} in the figure). It is thus possible to obtain oscillation in a semiconductor laser with active regions that are only a few tens of microns long. Commercial diode lasers have typical lengths of ~250 μm.

For additional background material on semiconductor lasers, the student is advised to consult References [10–12].

15.3 GaAs/$Ga_{1-x}Al_xAs$ LASERS

The two most important classes of semiconductor lasers are those that are based on III-V semiconductors. The first system is based on GaAs and $Ga_{1-x}Al_xAs$. The active region in this case is GaAs or $Ga_{1-x}Al_xAs$. The subscript x indicates the fraction of the Ga atoms in GaAs that are replaced by Al. The resulting lasers emit (depending on the active region molar fraction x and its doping) at $0.75\ \mu m < \lambda < 0.88\ \mu m$. This spectral region is convenient for the short-haul (<2 km) optical communication in silica fibers.

The second system has $Ga_{1-x}In_xAs_{1-y}P_y$ as its active region. The lasers emit in the $1.1\ \mu m < \lambda < 1.6\ \mu m$ depending on x and y. The region near 1.55 μm is especially favorable, since, as shown in Figure 3-12, optical fibers are available with losses as small as 0.15 dB/km at this wavelength, making it extremely desirable for long-distance optical communication.

In this section we will consider GaAs/$Ga_{1-x}Al_xAs$ lasers. A generic laser of this type, depicted in Figure 15-9, has a thin (0.1–0.2 μm) region of GaAs sandwiched between two regions of GaAlAs. It is consequently called a *double heterostructure* laser. The basic layered structure is grown epitaxially on a crystalline GaAs substrate so that it is uninterrupted crystalographically.

The favored crystal growth techniques are liquid-phase epitaxy and chemical vapor deposition using metallo-organic reagents (MOCVD) [11, 13, 14]. Another important technique—molecular beam epitaxy [11, 13, 15, 16]—uses atomic beams of the crystal constituents in ultra-high vacuum to achieve extremely fine thickness and doping control.

The thin active region is usually undoped while one of the bounding $Ga_{1-x}Al_xAs$ layers is doped heavily p-type and the other n-type. The difference

$$n_{GaAs} - n_{Ga_{1-x}Al_xAs} \simeq 0.62x$$

between the indices of refraction of GaAs and the ternary crystal with a molar fraction x gives rise to a three-layered dielectric waveguide of the type illustrated in Figure 13-1. At this point the student should review the basic modal concepts discussed in Chapter 13. The lowest-order (fundamental) mode has its energy concentrated mostly in the GaAs (high index) layer. The index distribution and a typical modal intensity plot for the lowest-order

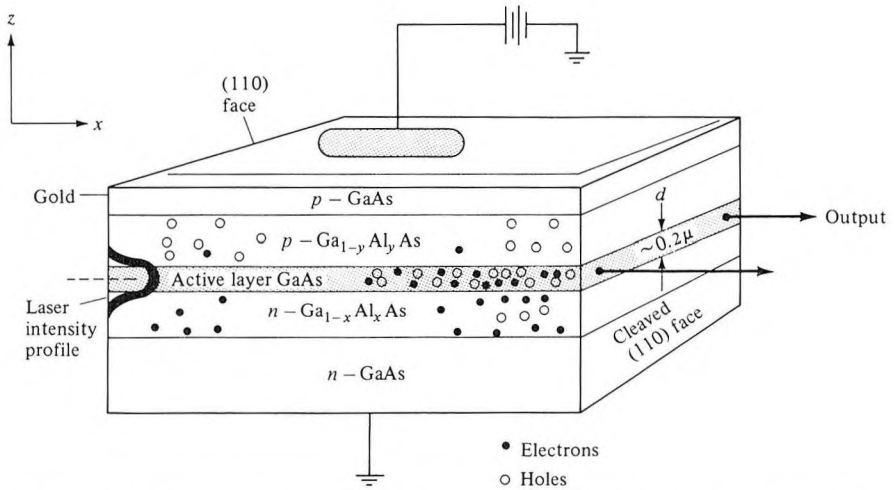

Figure 15-9 A typical double heterostructure GaAs-GaAlAs laser. Electrons and holes are injected into the active GaAs layer from the n and p GaAlAs. Frequencies near $\nu = E_g/h$ are amplified by stimulating electron–hole recombination.

mode are shown in Figure 15-10. When a positive bias is applied to the device, electrons are injected from the n-type $Ga_{1-x}Al_xAs$ into the active GaAs region while a density of holes equal to that of the electrons in the active region is caused by injection from the p side.

The electrons that are injected into the active region are prevented from diffusing out into the p region by means of the potential barrier due to the difference ΔE_g between the energy gaps of GaAs and $Ga_{1-x}Al_xAs$. The x-dependence of the energy gap is approximated by [13]

$$E_g(x < 0.37) = (1.424 + 1.247x) \text{ eV}$$

and is plotted in Figure 15-11.

The total discontinuity ΔE_g of the energy gap at a GaAs/GaAlAs interface is taken up mostly (60 percent) by the conduction band edge, while 40 percent is left to the valence band, so that both holes and electrons are effectively confined to the active region. This double confinement of injected carriers as well as of the optical mode energy to the same region is probably the single most important factor responsible for the successful realization of low-threshold continuous semiconductor lasers [17–19]. Under these conditions we expect the gain experienced by the mode to vary as d^{-1}, where d is the thickness of the active (GaAs) layer, since at a given total current the carrier density, hence the gain, will be proportional to d^{-1}. To quantify

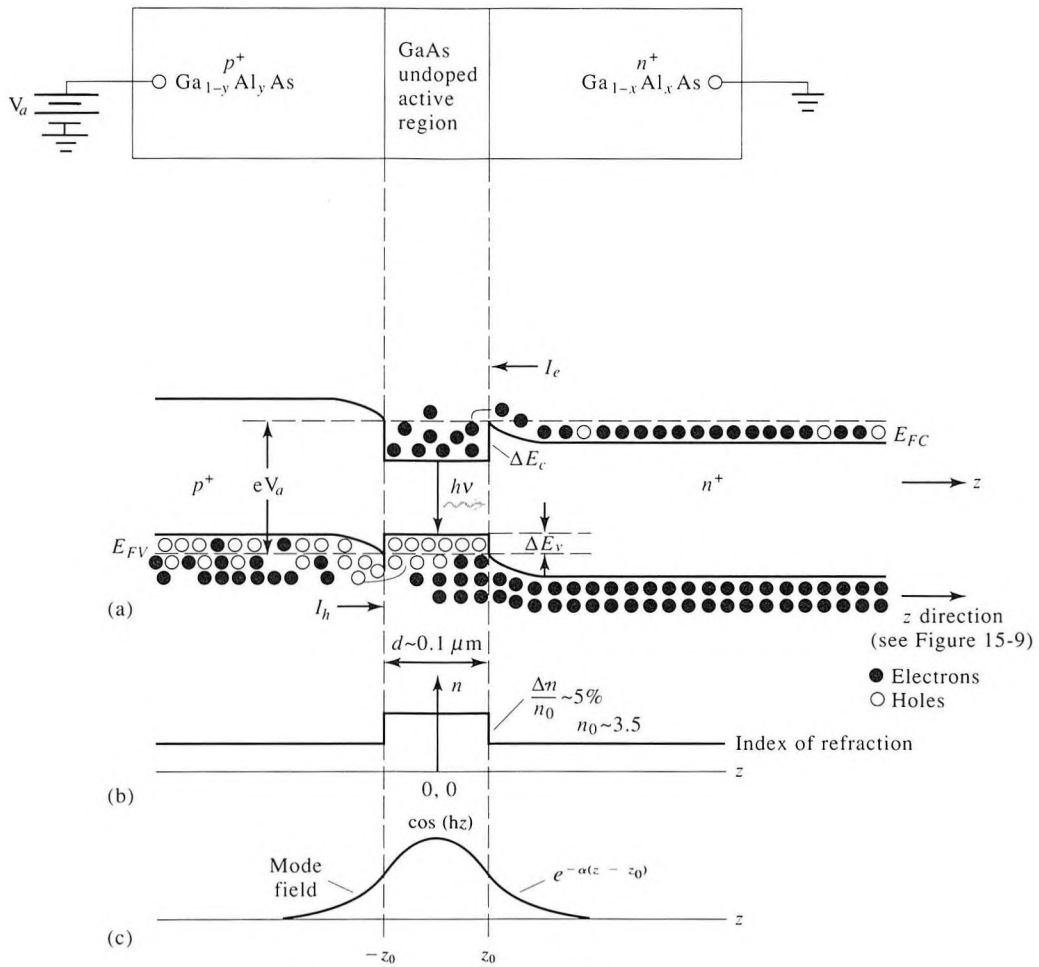

Figure 15-10 (a) The energy band edges of a strongly forward-biased (near-flattened) double heterostructure GaAs/GaAlAs laser diode. Note trapping of electrons (holes) in the potential well formed by the conduction (valence) band edge energy discontinuity $\Delta E_c(\Delta E_v)$. (b) The spatial (z) profile of the index of refraction which is responsible for dielectric waveguiding in the high index (GaAs) layer. (c) The intensity profile of the fundamental optical mode in a slab waveguide.

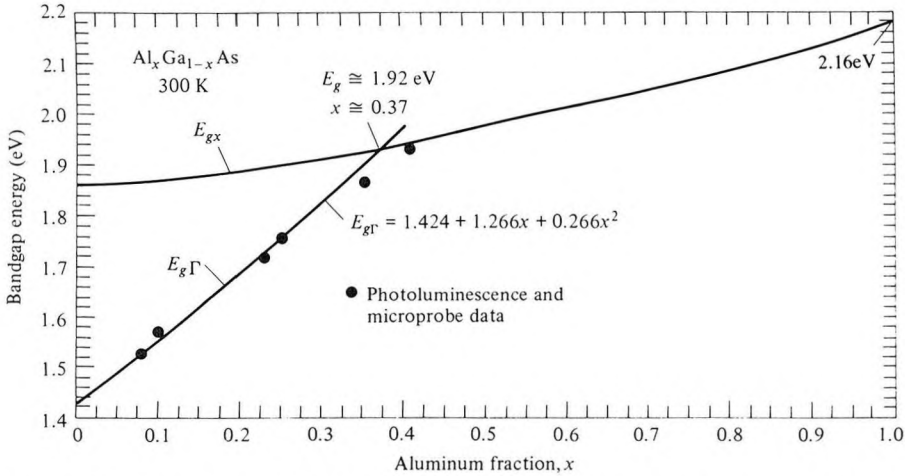

Figure 15-11 The magnitude of the energy gap in $Ga_{1-x}Al_xAs$ as a function of the molar fraction x. For $x > 0.37$ the gap is indirect. (After Reference [11].)

the last statement, we start with the basic definition of the modal gain

$$g = \frac{\text{power generated per unit length (in } x)}{\text{power carried by beam}} = \frac{-\int_{-\infty}^{-d/2} \alpha_n |E|^2 \, dz + \int_{-d/2}^{d/2} \gamma |E|^2 \, dz - \int_{d/2}^{\infty} \alpha_p |E|^2 \, dz}{\int_{-\infty}^{\infty} |E|^2 \, dz} \tag{15.3-1}$$

where γ is the gain constant experienced by a plane wave in a medium whose inversion density is equal to that of the active medium. γ is given by (15.2-12) and (15.2-17). α_n is the loss constant of the unpumped n-$Ga_{1-x}Al_xAs$ and is due mostly to free electron absorption. α_p is the loss (by free holes) in the bounding p-$Ga_{1-y}Al_yAs$ region. We note that as $d \to \infty$, $g \to \gamma$.

It is convenient to rewrite (15.3-1) as

$$g = \gamma\Gamma_a - \alpha_n\Gamma_n - \alpha_p\Gamma_p \tag{15.3-2}$$

$$\Gamma_a = \frac{\int_{-d/2}^{d/2} |E|^2 \, dz}{\int_{-\infty}^{\infty} |E|^2 \, dz} \tag{15.3-3a}$$

$$\Gamma_n = \frac{\int_{-\infty}^{-d/2} |E|^2 \, dz}{\int_{-\infty}^{\infty} |E|^2 \, dz} \tag{15.3-3b}$$

$$\Gamma_p = \frac{\int_{d/2}^{\infty} |E|^2 \, dz}{\int_{-\infty}^{\infty} |E|^2 \, dz} \tag{15.3-3c}$$

$$\Gamma_a + \Gamma_a + \Gamma_p = 1$$

Γ_a is very nearly the fraction of the mode power carried within the active GaAs layer, while Γ_n and Γ_p are, respectively, the fraction of the power in the n and p regions. As long as $\Gamma_a \sim 1$, i.e., most of the mode energy is in the active region, the gain g is inversely proportional to the active region thickness d since decreasing d, for example, increases the optical intensity for a given total beam power and, consequently, the rate of stimulated transitions. As d decreases, an increasing fraction of the mode intensity is carried outside the active region as can be seen from the modal waveguide solution plotted in Figure 15-12 [11]. The resulting decrease of the confinement factor Γ_a eventually dominates over the d^{-1}-dependence and the gain begins to decrease with further decrease of d [22]. A plot of the threshold current dependence on d is depicted in Figure 15-13. The bottoming out and eventual increase of J_{th} for $d \lesssim 0.1$ μm is due to the decrease of the confinement factor Γ_a and the increase of the relative role of the losses in the

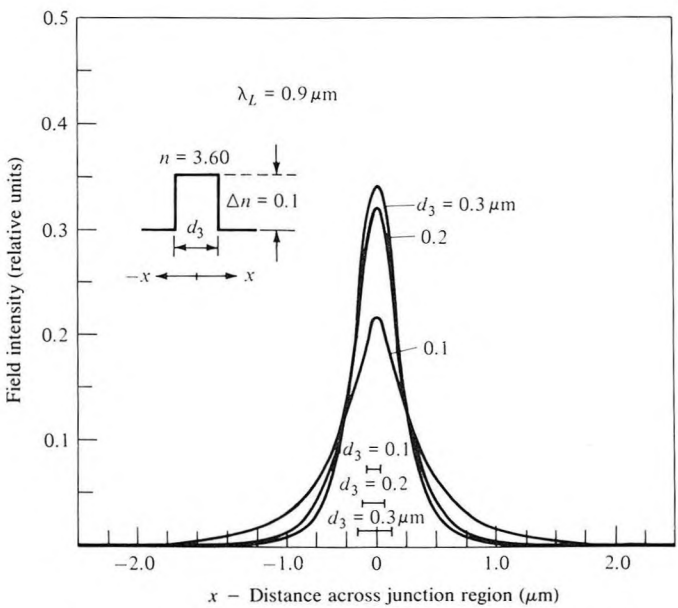

Figure 15-12 Calculated near field intensity distribution of the step discontinuity waveguide for various values of the guiding layer thickness. (After Reference [11].)

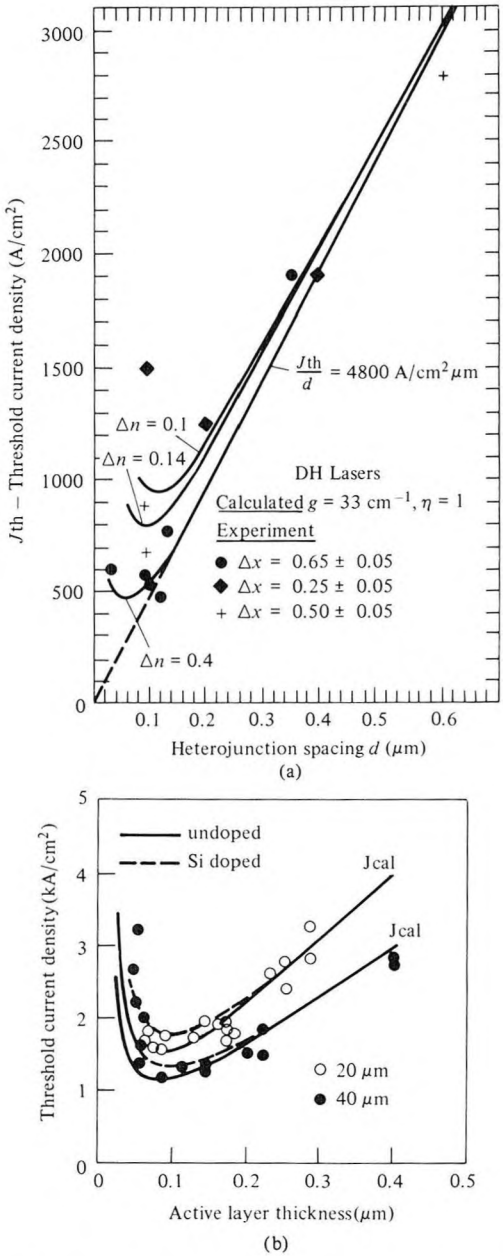

Figure 15-13 (a) Calculated and experimental values of the threshold current density as a function of the active layer thickness d for broad-area 500-μm-long AlGaAs DH diode lasers of "undoped" active layers. Notable exceptions are the experimental data for $\Delta x \simeq 0.25$, which were obtained from diodes with heavy-Ge-doped active layers. (After Reference [11].) (b) Calculated and experimental values of the threshold current density as a function of active layer thickness d for stripe-geometry (20- and 40-μm-wide stripe contacts) 300-μm-long AlGaAs DH diode lasers ($\Delta x = 0.25$) of "undoped" and low-Si-doped active layers ($x = 0.05$). (After Reference [21].)

p and n GaAlAs bounding layer as Γ_n and Γ_p increase, i.e., as an increasing fraction of the mode intensity is carried within these lossy unpumped regions as shown in Figure 15-12.

Numerical Example: Threshold Current Density in Double Heterostructure Lasers

Consider the case of a GaAs/GaAlAs laser of the type illustrated in Figure 15-10. We will use the following parameters: $\tau \sim 4 \times 10^{-9}$ s, $L = 500$ μm. The threshold gain condition is (15.3-2)

$$\gamma\Gamma_a = \alpha_n\Gamma_n + \alpha_p\Gamma_p - \frac{1}{L}\ln R + \alpha_s \tag{15.3-4}$$

where the term α_s accounts for scattering losses (mostly at heterojunction interfacial imperfections). The largest loss term in lasers with uncoated faces is usually $L^{-1} \ln R$. In our case, taking $R = 0.31$ as due to Fresnel reflectivity at a GaAs ($n = 3.5$) air interface, we obtain

$$-\frac{1}{L}\ln R = 23.4 \text{ cm}^{-1}$$

The rest of the loss terms are assumed to add up to ~ 10 cm^{-1} so that taking $\Gamma_a \sim 1$ the total gain needed is 33.4 cm^{-1}. This requires, according to Figure 15-8, an injected carrier density of $N \sim 1.7 \times 10^{18}$ cm^{-3}. Under steady-state conditions the rate at which carriers are injected into the active region must equal the electron–hole recombination rate

$$\frac{J}{e} = \frac{Nd}{\tau}$$

Using the above data we obtain

$$\frac{J}{d} = \frac{eN}{\tau} \sim 6.8 \times 10^3 \text{ A/(cm}^2\text{-}\mu\text{m)}$$

This value of J/d is in reasonable agreement with the measured value of $\sim 5 \times 10^3$ in Figure 15-13. If we use this value to estimate the lowest threshold current density which from Figure 15-13 occurs when $d \sim 0.08$ μm, we obtain

$$J_{\min} = 0.68 \times 10^4 \times 0.08 = 544 \text{ A/cm}^2$$

again, close to the range of observed values.

The successful epitaxial growth of $Ga_{1-x}Al_xAs$ on top of GaAs (and vice versa), which is the main reason for the success of double heterostructure

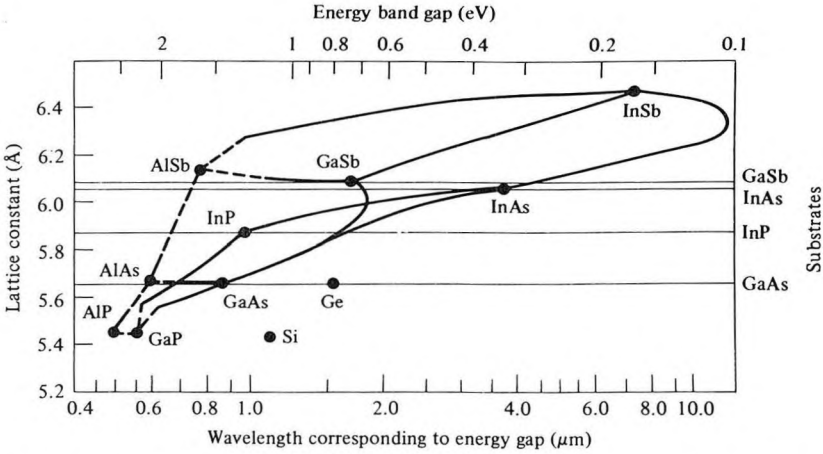

Figure 15-14 III-V compounds: Lattice constants versus energy band gaps and corresponding wavelengths. The solid lines correspond to direct-gap materials and the dashed lines to indirect-gap materials. The binary-compound substrates that can be used for lattice-matched growth are indicated on the right. [After Reference [11].)

lasers, is due to the fact that their lattice constants are the same, to within a fraction of a percent, over the range $0 \leq x \leq 1$. This can be seen from the plot of Figure 15-14, which shows the lattice constant corresponding to various compositions of III-V semiconductors as a function of the band gap energy. We note that the line connecting the AlAs ($x = 1$) and the GaAs($x = 0$) is nearly horizontal, which corresponds to a (very nearly) constant lattice constant over this compositional range.

15.4 SOME REAL LASERS

The double heterostructure lasers discussed in Section 15.3 lack the means for confining the current and the radiation in the lateral (y) direction. The outcome is that typical broad area lasers can support more than one transverse (y) mode, resulting in unacceptable mode hopping as well as spatial and temporal instabilities. To overcome these problems, modern semiconductor lasers employ some form of transverse optical and carrier confinement. A typical and successful example of this approach is the buried heterostructure laser [20] shown in Figure 15-15. To fabricate these lasers, the first three layers: n-$Ga_{1-x}Al_xAs$, GaAs, and p-$Ga_{1-y}Al_yAs$ are grown on a n-GaAs crystalline substrate by one of the epitaxial techniques described above. The structure is then etched through a mask down to the substrate

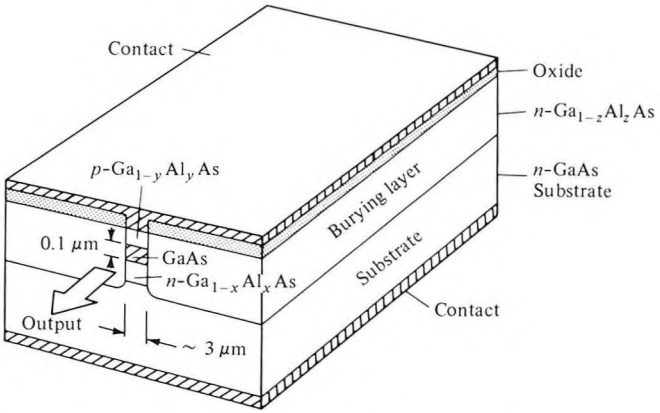

Figure 15-15 A buried heterostructure laser [20].

level, leaving stand a thin (~3 μm) rectangular mesa composed of the original layers. A "burying" $Ga_{1-z}Al_zAs$ layer is then regrown on both sides of the mesa, resulting in the structure shown in Figure 15-15.

The most important feature of the buried heterostructure laser is that the active GaAs region is surrounded on *all* sides by the lower index GaAlAs, so that electromagnetically the structure is that of a rectangular dielectric waveguide. The transverse dimensions of the active region and the index discontinuities (i.e., the molar fractions x, y, and z) are so chosen that only the lowest-order transverse mode can propagate in the laser waveguide. Another important feature of this laser is the confinement of the injected carriers at the boundaries of the active region due to the energy band discontinuity at a GaAs/GaAlAs interface as discussed in the last section. These act as potential barriers inhibiting carrier escape out of the active region. GaAs semiconductor lasers utilizing this structure have been fabricated, see Chapter 16, with threshold currents of less than 1 milliampere [38]; more typical lasers have thresholds of ~20 milliamperes.

Power Output of Injection Lasers

The considerations of saturation and power output in an injection laser are basically the same as that of conventional lasers, which were described in Section 5.5. As the injection current is increased above the threshold value, the laser oscillation intensity builds up. The resulting stimulated emission shortens the lifetime of the inverted carriers to the point where the magnitude of the inversion is clamped at its threshold value. Taking the probability that

an injected carrier recombine radiatively within the active region as η_i,[2] we can write the following expression for the power emitted by stimulated emission:

$$P_e = \frac{(I - I_t)\eta_i}{e} h\nu \tag{15.4-1}$$

Part of this power is dissipated inside the laser resonator, and the rest is coupled out through the end reflectors. These two powers are, according to (15.3-4), proportional to the effective internal loss $\alpha \equiv \alpha_n\Gamma_n + \alpha_p\Gamma_p + \alpha_s$ and to $-L^{-1} \ln R$, respectively. We can thus write the output power as

$$P_0 = \frac{(I - I_t)\eta_i h\nu}{e} \frac{(1/L) \ln (1/R)}{\alpha + (1/L) \ln (1/R)} \tag{15.4-2}$$

The external differential quantum efficiency η_{ex} is defined as the ratio of the photon output rate that results from an increase in the injection rate (carriers per second) to the increase in the injection rate:

$$\eta_{ex} = \frac{d(P_0/h\nu)}{d[(I - I_t)/e]} \tag{15.4-3}$$

Using (15.4-2) we obtain

$$\eta_{ex}^{-1} = \eta_i^{-1} \left(\frac{\alpha L}{\ln (1/R)} + 1 \right) \tag{15.4-4}$$

By plotting the dependence of η_{ex} on L we can determine η_i, which in GaAs is around 0.9–1.0.

Since the incremental efficiency of converting electrons into useful output photons is η_{ex}, the main remaining loss mechanisms degrading the conversion of electrical to optical power is the small discrepancy between the energy eV_{appl} supplied to each injected carrier and the photon energy $h\nu$. This discrepancy is due mostly to the series resistance of the laser diode. The efficiency of the laser in converting electrical power input to optical power is thus

$$\eta = \frac{P_0}{VI} = \eta_i \frac{I - I_t}{I} \frac{h\nu}{eV_{appl}} \frac{\ln (1/R)}{\alpha L + \ln (1/R)} \tag{15.4-5}$$

In practice $eV_{appl} \sim 1.4E_g$ and $h\nu \simeq E_g$. Values of $\eta \sim 30$ percent at 300 K have been achieved.

We conclude this section by showing in Figures 15-16 and 15-17 typical plots of the power output versus current and the far field of commercial low-threshold GaAs semiconductor lasers.

---

[2]The reason for a quantum efficiency η_i that is less than unity is, mostly, the existence of a leakage current component that bypasses the active p-n junction region.

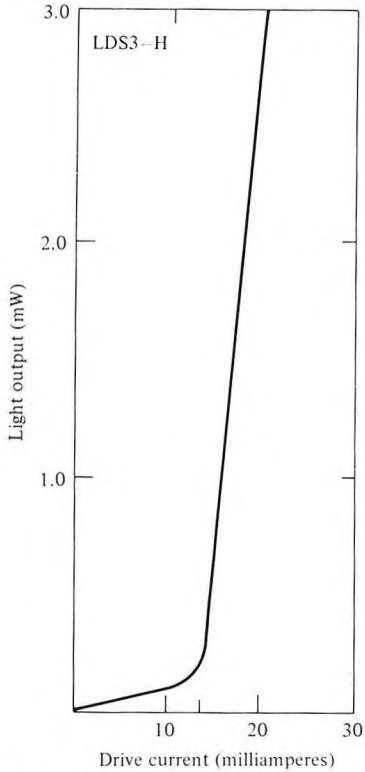

Figure 15-16 Power versus current plot of a low-threshold (~14 milliamperes) commercial DH GaAs/GaAlAs laser. (After Reference [23].)

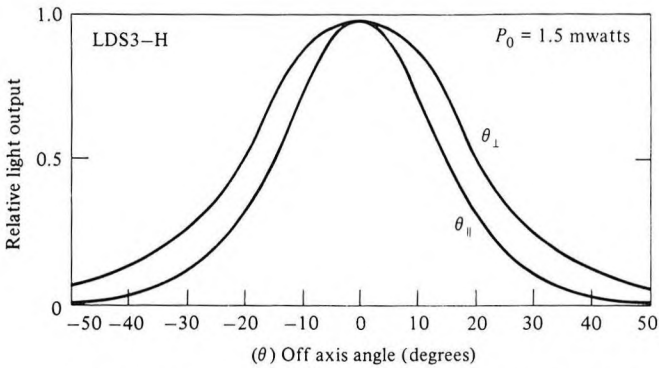

Figure 15-17 Far-field angular intensity distribution of a low-threshold commercial DH GaAs/GaAlAs laser. (After Reference [23].)

15.5 GaInAsP LASERS

Semiconductor lasers that utilize an active region of the quaternary semiconductor $Ga_{1-x}In_xAs_{1-y}P_y$ and bounding layers of InP are of great technological importance [24]. A drawing of a buried heterostructure laser based on this system is shown in Figure 15-18. According to Figure 15-14, it is possible to match the lattice constant of the InP substrate to that of $Ga_{1-x}In_xAs_{1-y}P_y$ over the (equivalent band gap energy) wavelength region $1.0\ \mu m < \lambda < 1.7\ \mu m$. From the absorption data of silica fiber in Figure 3-12, we see that this wavelength regime includes some of the low-loss regions of silica fibers.

Another fortunate circumstance favoring optical communication in this wavelength region is the possibility of designing fibers in such a way that the chromatic (n versus λ) and waveguide dimensional group velocity dispersion cancel each other to first order in the 1.3-μm (or 1.5-μm) region so that extremely short optical pulses can propagate long distances with minimal spreading as discussed in Section 3.6. This has made GaInAsP/InP semiconductor lasers the preferred optical sources for long-distance optical communication via fibers [26].

Recent experiments have demonstrated optical links ~150 km long without repeaters in the 1.55-μm region. For a review of this important area, the reader should consult Reference [26] and the many citations quoted therein.

15.6 DIRECT-CURRENT MODULATION OF SEMICONDUCTOR LASERS

Since the main application of semiconductor lasers is as sources for optical communication systems, the problem of high-speed modulation of their output by the high-data-rate information is one of great technological importance.

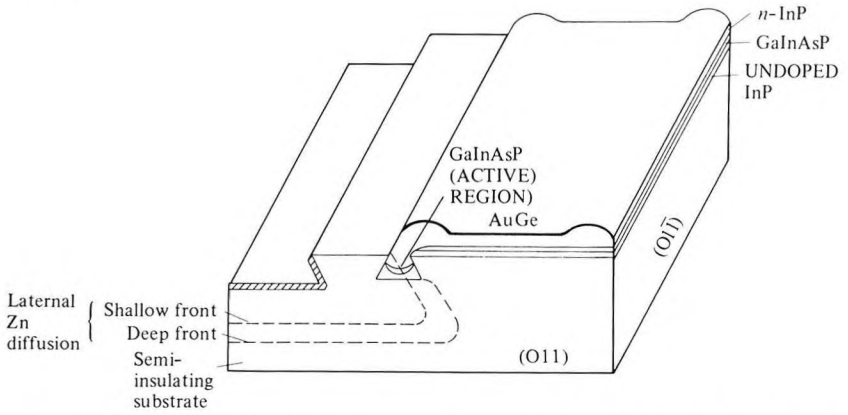

Figure 15-18 An embedded crescent-shaped active region GaInAsP/InP laser. (After Reference [25].)

A unique feature of semiconductor lasers is that, unlike other lasers that are modulated externally (see Chapter 9), the semiconductor laser can be modulated directly by modulating the excitation current. This is especially important in view of the possibility of monolithic integration of the laser and the modulation electronic circuit, as will be discussed in Section 15.7. The following treatment follows closely that of Reference [27].

If we denote the photon density inside the active region of a semiconductor laser by P and the injected electron (and hole) density by N, then we can write

$$\frac{dN}{dt} = \frac{I}{eV} - \frac{N}{\tau} - A(N - N_{tr})P$$
$$\frac{dP}{dt} = A(N - N_{tr})P\Gamma_a - \frac{P}{\tau_p} \tag{15.6-1}$$

where I is the total current, V the volume of the active region, τ the spontaneous recombination lifetime, τ_p the photon lifetime as limited by absorption in the bounding media, scattering and coupling through the output mirrors.

The term $A(N - N_{tr})P$ is the net rate per unit volume of induced transitions. N_{tr} is the inversion density needed to achieve transparency as defined by (15.2-17), and A is a temporal growth constant that by definition is related to the constant B defined by (15.2-17) by the relation $A = Bc/n$. Γ_a is the filling factor defined by (15.3-3), and its presence here is merely a matter of bookkeeping to ensure that the total number, rather than the density variables used in (15.6-1), of electrons undergoing stimulated transitions is equal to the number of photons emitted. The contribution of spontaneous emission to the photon density is neglected since only a very small fraction ($\sim 10^{-4}$) of the spontaneously emitted power enters the lasing mode.

By setting the left side of (15.6-1) equal to zero, we obtain the steady-state solutions N_0 and P_0

$$0 = \frac{I_0}{eV} - \frac{N_0}{\tau} - A(N_0 - N_{tr})P_0$$
$$0 = A(N_0 - N_{tr})P_0\Gamma_a - \frac{P_0}{\tau_p} \tag{15.6-2}$$

We consider the case where the current is made up of dc and ac components ($i\omega_m t$)

$$I = I_0 + i_1 e^{i\omega_m t} \tag{15.6-3}$$

and define the small-signal modulation response n_1 and p_1 by

$$N = N_0 + n_1 e^{i\omega_m t} \qquad P = P_0 + p_1 e^{i\omega_m t} \tag{15.6-4}$$

where N_0 and P_0 are the dc solutions of (15.6-2).

Using (15.6-3), (15.6-4), and the result $A(N_0 - N_{tr}) = (\tau_p \Gamma_a)^{-1}$ from (15.6-2) in (15.6-1) leads to the small-signal algebraic equations

$$-i\omega_m n_1 = -\frac{i_1}{eV} + \left(\frac{1}{\tau} + AP_0\right) n_1 + \frac{1}{\tau_p \Gamma_a} p_1$$

$$i\omega_m p_1 = AP_0 \Gamma_a n_1 \qquad (15.6\text{-}5)$$

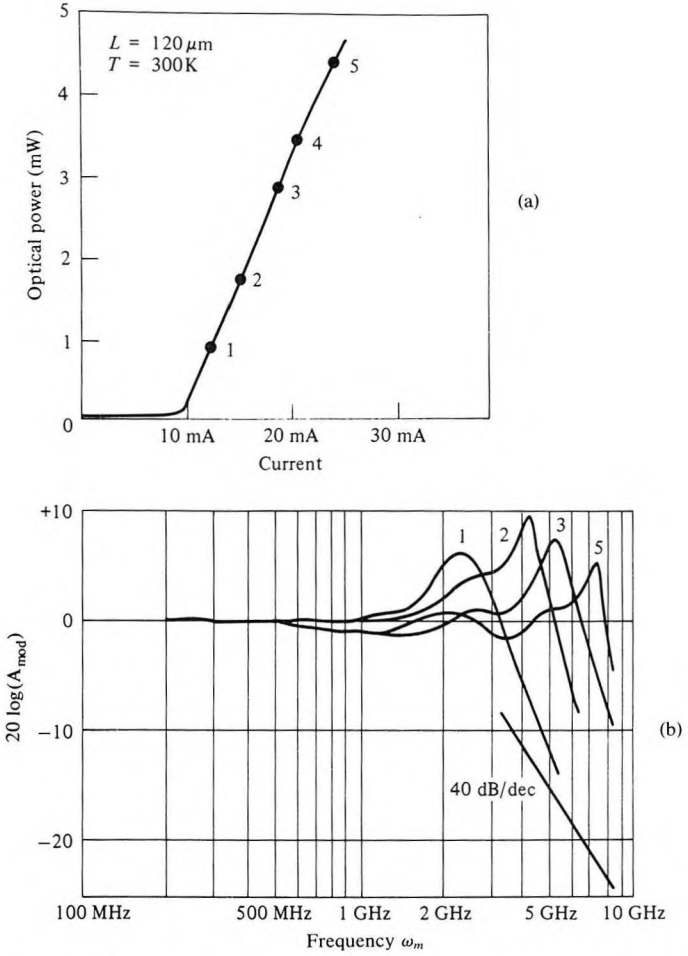

Figure 15-19 (a) *CW* light output power versus current characteristic of a laser of length = 120 μm. (b) Modulation characteristics of this laser at various bias points indicated in the plot. (c) Measured relaxation oscillation resonance frequency of lasers of various cavity lengths as a function of $\sqrt{P}$, where P is the cw output optical power. The points of catastrophic damage are indicated by downward pointing arrows. (After Reference [27].)

Our main interest is in the modulation response $p_1(\omega_m)/i_1(\omega_m)$ so that from (15.6-5) we obtain

$$p_1(\omega_m) = \frac{-(i_1/eV)AP_0\Gamma_a}{\omega_m^2 - i\omega_m/\tau - i\omega_m AP_0 - AP_0/\tau_p} \tag{15.6-6}$$

A typical measurement of $p_1(\omega_m)$ is shown in Figure 15-19(b). The response curve is flat at small frequencies peaks at the "relaxation resonance frequency" ω_R and then drops steeply. The peaking is due to the same mechanism as that causing the relaxation resonance of conventional lasers that was discussed in Section 6.9. The expression for the peak frequency is obtained by minimizing the magnitude of the denominator of (15.6-6)

$$\omega_R = \sqrt{\frac{AP_0}{\tau_p} - \frac{1}{2}\left(\frac{1}{\tau} + AP_0\right)^2} \tag{15.6-7}$$

In a typical semiconductor laser with $L = 300\ \mu$m, we have from (4.7-3) $\tau_p \simeq (n/c)(\alpha - (1/L)\ln R)^{-1} \sim 10^{-12}$ s, $\tau \sim 4 \times 10^{-9}$ s, and $AP_0 \sim 10^9\ s^{-1}$ so that to a very good accuracy

$$\omega_R = \sqrt{\frac{AP_0}{\tau_p}} \tag{15.6-8}$$

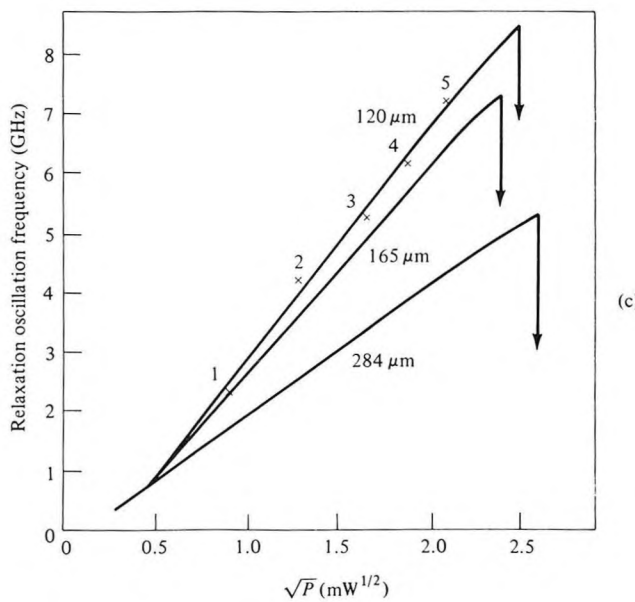

(c)

The last result is extremely useful, since it suggests that to increase ω_R and thus increase the useful linear region of the modulation response $p_1(\omega_m)/i_1(\omega_m)$, we need to increase the optical gain coefficient A, decrease the photon lifetime τ_p, and operate the laser at as high internal photon density P_0 as possible. A detailed discussion of the optimum strategy for maximizing ω_R is given in Reference [27].

It is somewhat tedious but straightforward to show that (15.6-8) can also be written as

$$\omega_R = \sqrt{\frac{1 + A\tau_p\Gamma N_{tr}}{\tau\tau_p}\left(\frac{I_0}{I_{th}} - 1\right)} \tag{15.6-9}$$

a result that is cast in a form similar to that of (6.9-14) except that here $A\tau_p\Gamma N_{tr} > 1$.

Numerical Example: Modulation Bandwidth in GaAs/GaAlAs Lasers

Here, using (15.6-8), we will estimate the uppermost useful modulation frequency ω_R of a typical GaAs/GaAlAs laser. We shall assume a typical laser emitting 5×10^{-3} watt from a single face with an active area cross section of 3 μm $\times$ 0.1 μm, a facet reflectivity of $R = 0.31$ and an index of refraction $n_0 = 3.5$. Solving for P_0 from the relationship

$$\frac{(1 - R)P_0 ch\nu}{n_0} = \frac{\text{power}}{\text{area}}$$

we obtain $P_0 = 1.21 \times 10^{15}$ photons/cm^3 for the photon density in the laser cavity. The constant A has a typical value of 2×10^{-6} cm^3/s. [This can be checked against the relationship $A = Bc/n_0$, where B is the spatial gain parameter of (15.2-17).] The photon lifetime τ_p is obtained from (4.7-3)

$$\tau_p = \frac{n_0}{c}\left(\alpha_{ab} - \frac{1}{L}\ln R\right)^{-1}$$

which for $L = 120$ μm, $\alpha_{ab} = 10$ cm^{-1}, and $R = 0.31$ yields $\tau_p \sim 1.08 \times 10^{-12}$ s. Combining these results gives

$$\nu_R \equiv \frac{\omega_R}{2\pi} = \frac{1}{2\pi}\sqrt{\frac{AP_0}{\tau_p}} = \frac{1}{2\pi}\sqrt{\frac{2 \times 10^{-6} \times 1.2 \times 10^{15}}{1.08 \times 10^{-12}}}$$
$$= 7.53 \times 10^9 \text{ Hz}$$

This value is in the range of the experimental data shown in Figure 15-19, which was obtained on a laser with characteristics similar to that used in our example. The square root law dependence of ω_R on the photon density (or power output) predicted by (15.6-8) is verified by the data of Figure 15-19(c).

The above example indicates the feasibility of direct modulation of semiconductors at up to microwave frequencies and hence of sending microwave signals riding piggyback on optical beams in fibers or space [28].

Density Modulation and Dynamic Frequency Chirping

In the first part of this section we found that a modulation of the injection current

$$I = I_0 + i_1 e^{i\omega_m t} \tag{15.6-10}$$

of a semiconductor laser leads to a modulation of the carrier density so that

$$N = N_0 + n_1 e^{i\omega_m t} \tag{15.6-11}$$

The amplitude n_1 of the carrier density fluctuations is obtained from (15.6-5) and (15.6-6)

$$n_1(\omega_m) = -i\left(\frac{i_1}{\mathrm{eV}}\right) \frac{\omega_m}{\omega_m^2 - \dfrac{AP_0}{\tau_p} - i\omega_m\left(\dfrac{1}{\tau} + AP_0\right)} \tag{15.6-12}$$

Recalling the definition $\omega_R^2 = AP_0/\tau_p$ and using the numerical values for AP_0, τ_p, and τ given above, we can write, for $\omega_R^2 \gg \omega_m/\tau$, $\omega_m AP_0$

$$n_1(\omega_m \ll \omega_R) = i\left(\frac{i_1}{\mathrm{eV}}\right)\frac{\omega_m}{\omega_R^2}$$

$$n_1(\omega_m = \omega_R) = \left(\frac{i_1}{\mathrm{eV}}\right)\frac{1}{\omega_R^2 \tau_p} \tag{15.6-13}$$

The general behavior of $n_1(\omega_m)$ is shown in Figure 15-20(a). $n_1(\omega_m)$ peaks at $\omega_m = \omega_R$.

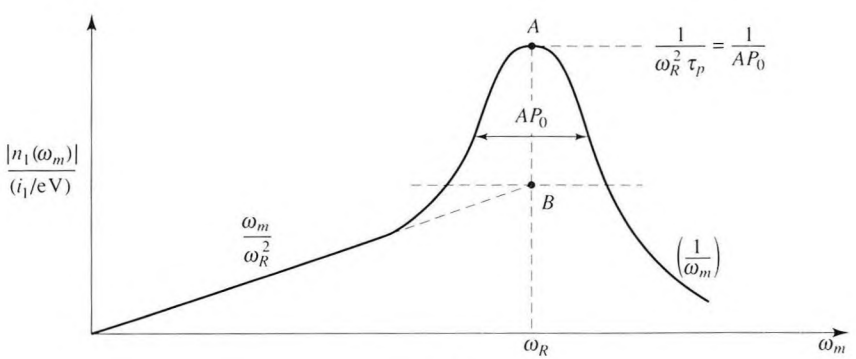

(a)

Figure 15-20 (a) A theoretical plot of the carrier density modulation n_1 as a function of the current modulation frequency ω_m. (b) (1) A scanning Fabry–Perot spectrum of a GaInAsP ($\lambda = 1.31\ \mu$m) DFB laser with no current modulation. (2) The spectrum of the same laser when the current is modulated at $f_m = 550$ MHz, horiz. scale = 1 GHz/div. (Courtesy of H. Blauvelt, P. C. Chen, and N. Kwong of ORTEL Corporation, Alhambra, California)

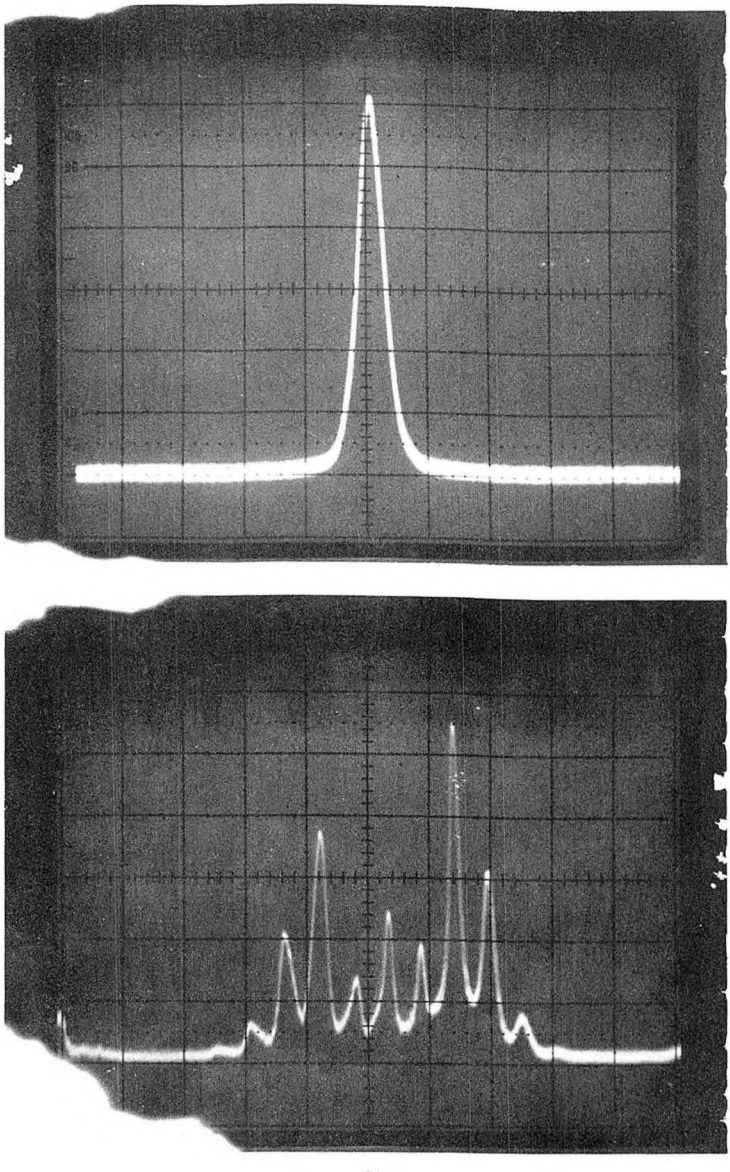

(b)

Figure 15-20 (*continued*)

Since the index of refraction of the active medium depends on the carrier density, a modulation $n_1 e^{i\omega_m t}$ of the carrier density of the semiconductor causes a modulation of the index of refraction n_0 of the active medium. Taking the index as

$$n_0 = n_0' + \mathrm{i}n_0'' \tag{15.6-14}$$

The carrier modulation as in (15.6-11) leads in first order to

$$n_0(t) = (n_0' + in_0'') + (\Delta n_0' + i\Delta n_0'')e^{i\omega_m t} \tag{15.6-15}$$

where $\Delta n_0'$ and $\Delta n_0''$ are the (complex) amplitudes of the modulation of the real and imaginary parts of n_0, respectively. Assuming that the oscillation frequency adjusts instantaneously to the value of n_0', we can express the change of the oscillation frequency due to a change $\Delta n_0'$

$$\frac{\Delta \nu}{\nu} = -\frac{\Delta n_0'}{n_0'}\Gamma_a \tag{15.6-16}$$

where the filling factor, $\Gamma_a \approx$ volume of active region/mode volume, accounts in an obvious way for the dependence of $\Delta\nu$ on the volume of the active region. Now consider a perturbation Δn in the carrier density. A little thought and scribbling shows that the differential gain constant A can be written as

$$A = \frac{4\pi\nu}{n_0'}\frac{\Delta n_0''}{\Delta n} \tag{15.6-17}$$

Another key parameter of semiconductor lasers is the α parameter defined in Section 10.7. It is the ratio of the change in the real part of n_0 to that of the imaginary part.

$$\alpha = \frac{\Delta n_0'}{\Delta n_0''} \tag{15.6-18}$$

α can be viewed as a material parameter that depends on temperature as well as on the carrier density. Its value in typical room temperature semiconductor lasers is $3 < |\alpha| < 6$ [34]. Combining the last two results we obtain

$$\Delta n_0' = \frac{\alpha n_0' A}{4\pi\nu}\Delta n \tag{15.6-19}$$

for the relation between the changes in the carrier density (Δn) and the index n_0'. In the case of the sinusoidal current modulation, we define $\Delta n = n_1 \exp(i\omega_m t)$ so that [34, 35] using (15.6-16),

$$\Delta\nu(t) = i\left(\frac{i_1}{\mathrm{eV}}\right)\frac{\Gamma_a A\alpha\omega_m e^{i\omega_m t}}{4\pi\left[\omega_m^2 - \dfrac{AP_0}{\tau_p} - i\omega_m\left(\dfrac{1}{\tau} + AP_0\right)\right]} \tag{15.6-20}$$

In most practical situations the applied modulation frequency ω_m satisfies the condition $\omega_m \ll \omega_R$ ($\equiv \sqrt{AP_0/\tau_p}$). Since this condition leads to a flat amplitude modulation response [see Figure 15-19(b)], in this case (15.6-20) becomes

$$\Delta\nu(t) = -i\frac{\Gamma_a A\alpha}{4\pi\mathrm{eV}}\left(\frac{\omega_m}{\omega_R^2}\right) i_1 e^{i\omega_m t}$$

$$\omega_m \ll \omega_R \tag{15.6-21}$$

The sinusoidal current modulation $i_1 \exp(i\omega_m t)$ thus causes, to first order, a frequency modulation. The sinusoidal frequency modulation should cause the optical spectrum to acquire (FM) sidebands occupying a spectral width

$$(\Delta\nu)_{\text{chirp}} \approx |\Delta\nu(t)_{\max}| = \frac{\Gamma_a A\alpha}{4\pi e V}\frac{\omega_m}{\omega_R^2} i_1 \qquad (15.6\text{-}22)$$

Example: Chirp Linewidth in a Modulated Semiconductor Laser

To estimate the spectral broadening expected in a semiconductor laser under typical current modulation conditions, consider the following case:

$\lambda = 0.84\ \mu\text{m}$ $\quad n_0' = 3.5$

$P = 5 \times 10^{-3}$ watts per facet

Cross section of active region $\quad 3\ \mu\text{m} \times 0.1\ \mu\text{m}$

R = facet reflectivity = 0.31 $\quad \alpha_{\text{abs}} = 10\ \text{cm}^{-1}$

$A = 2 \times 10^{-6}\ \text{cm}^3/\text{s} = 2 \times 10^{-12}\ \text{m}^3/\text{s}$

Length of active region $\quad 120\ \mu\text{m}$

These data were used earlier in this section to obtain the following results:

$$P_0 = 1.21 \times 10^{15}\ \text{photons/cm}^3$$

$$\frac{\omega_R}{2\pi} = 7.53 \times 10^9\ \text{Hz}$$

If we assume in addition $\alpha = 4$, $\Gamma_a = 0.5$, with a modulation current of $i_1 = 5$ mA at a modulation frequency of $\omega_m/2\pi = 5 \times 10^8$ Hz, we obtain from (15.6-21) that the chirped linewidth is

$$(\Delta\nu)_{\text{chirp}} \cong 4 \times 10^8\ \text{Hz}$$

Figure 15-20(b) shows the field spectrum of a semiconductor laser with and without current modulation. Note the nearly order-of-magnitude increase of the spectral region occupied by the laser field with modulation. This increase in spectral width conspires with the group velocity dispersion of fibers and causes broadening of pulses propagating in these fibers. This limits the maximum rate of data transmission as discussed in Section 2.9. The quest for a spectrally narrow semiconductor laser is an active area of research.

15.7 INTEGRATED OPTOELECTRONICS

In one of its rare moments of cooperative spirit, nature has endowed the III-V semiconductors based on GaAs/GaAlAs and InP/GaInAsP with a double gift. These are, as discussed above, the materials of choice for semiconductor lasers, but in addition it is possible to use them, especially GaAs/GaAlAs, as base materials for electronic circuits in a manner similar to that in silicon.[3]

It was pointed out in 1971 [30] that it should be possible to bring together monolithically in a III-V semiconductor the two principal actors of the modern communication era—the transistor and the laser—in new integrated optoelectronic circuits. This new technology is now taking its first tentative steps from the laboratory to applications.

The basic philosophy, as well as an example of an integrated optoelectronic device, is shown in Figure 15-21, which shows a buried heterostructure GaAs/GaAlAs laser, similar to that illustrated in Figure 15-15, fabricated monolithically on the same crystal as a field-effect transistor (FET). The output current of the FET (see arrows) supplies the electron injection to the active region of the laser. This current and thus the laser power output can be controlled by a bias voltage applied to the gate electrode.

An example of a feasibility model of an integrated optoelectronic optical repeater, which incorporates a detector, a FET current preamplifier, a FET laser driver, and a laser, is shown in Figure 15-22. The main reason for the accelerating drive toward an integrated optoelectronic circuit technology [33] derives from the reduction of parasitic reactances that are always as-

[3] A completely new electronic technology based on GaAs/GaAlAs is now emerging [29]. It takes advantage of the large mobility of electrons in GaAs for very high switching speeds.

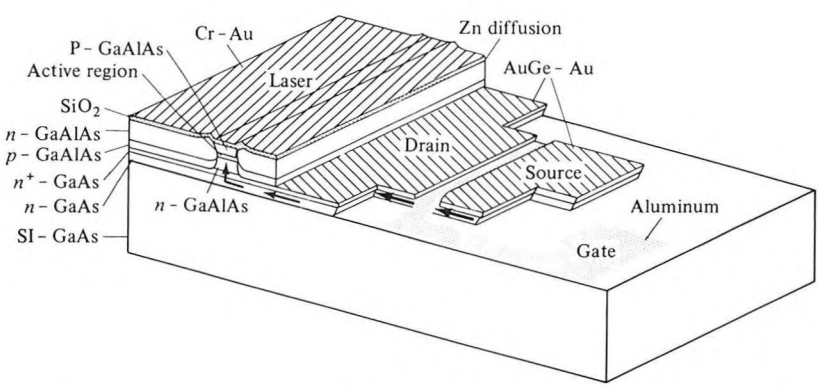

Figure 15-21 A GaAs n-channel field-effect transistor integrated monolithically with a buried heterostructure GaAs/GaAlAs laser. The application of a gate voltage is used to control the bias current of the laser. This voltage can oscillate and modulate the light at frequencies > 10 GHz. (After Reference [31].)

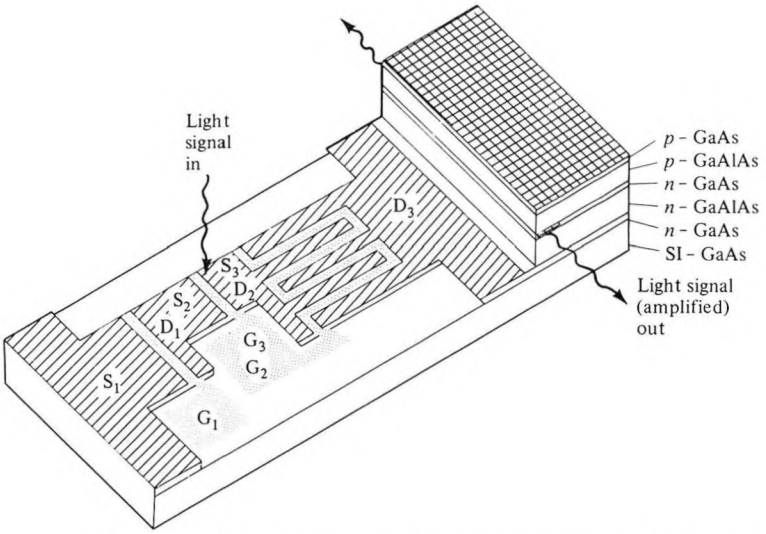

Figure 15-22 A monolithically integrated optoelectronic repeater containing a detector, transistor current source, a FET amplifier, and a laser on a single crystal GaAs substrate. (After Reference [32].)

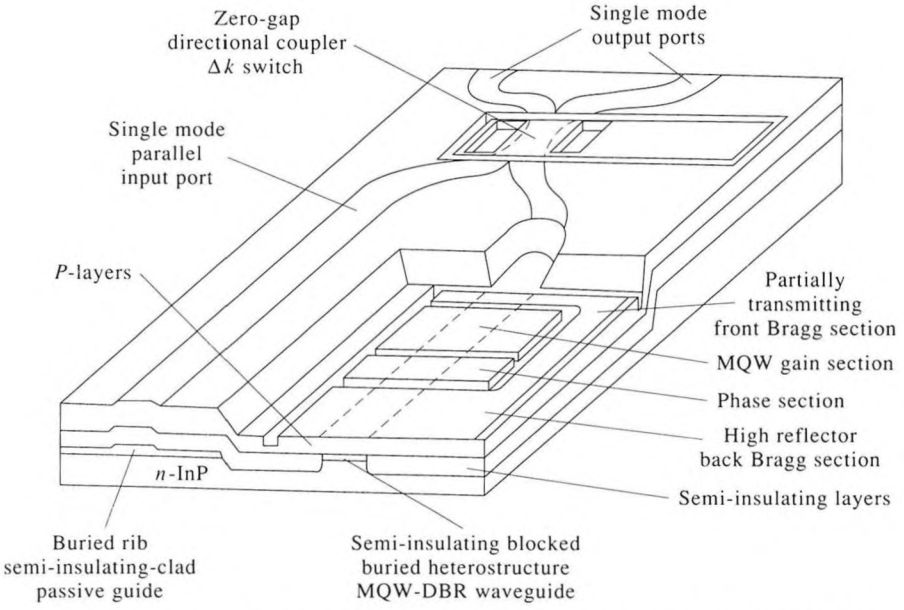

Figure 15-23 A monolithic circuit containing a tunable multisection InGaAsP/InP 1.55 μm laser employing multiquantum well gain section, a passive waveguide for an external input optical wave, and a directional coupler switch for combining the laser output field and that of the external input at the output ports. (After Reference [34].)

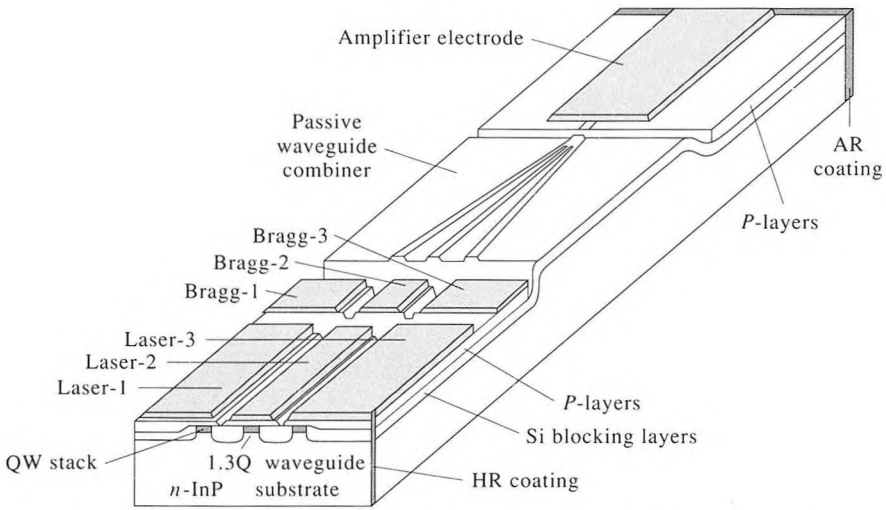

Figure 15-24 An optoelectronic integrated circuit composed of three ~1.5 μm InGaAs/InP distributed feedback lasers each tuned to a slightly different wavelength. The three wavelengths are fed into a single waveguide and amplified in a single amplifying section. (After Reference [35].)

sociated with conventional wire interconnections, plus the compatibility with the integrated electronic circuits technology that makes it possible to apply the advanced techniques of the latter to this new class of devices. More recent examples of optoelectronic integrated circuits are demonstrated in Figures 15-23 and 15-24.

Problems

15.1 Derive Equations (15.6-12) and (15.6-17).

15.2 Using the theory of phase modulation, show that the frequency modulation (15.6-21) leads to a spectral width as given by (15.6-22). [*Hint*: Use the fact that if $E(t) = E_0 \cos(\omega t + \delta \cos \omega_m t)$ the Bessel series expansion of $E(t)$ contains appreciable sidebands up to order $n \approx \delta$.]

15.3 Assume a fiber with $L = 10$ km and a group velocity dispersion parameter of 10 psec/nm-km (see Section 3.3). Calculate the maximum data rate through the fiber in bits/s if we use a semiconductor laser with characteristics similar to those used in the example of Section 15.6. For the purpose of this calculation, assume that a data rate of N bits/s is equivalent to a current modulation frequency of $\omega_m/2\pi = N$.

15.4 Derive relation (15.6-20).

15.5 Evaluate and plot:

(a) The gain $\gamma(\omega)$ of an inverted GaAs crystal under the following conditions:

$$N_{\text{elec}} = N_{\text{hole}} = 3 \times 10^{18}\ \text{cm}^{-3}$$
$$m_c = 0.07\ m_{\text{electron}}$$
$$m_h = 0.4\ m_{\text{electron}}$$
$$T = 0\ \text{K}$$
$$E_g = 1.45\ \text{eV}$$
$$T_2 = \infty$$

(b) Comment qualitatively on the changes in $\gamma(\omega)$ as the temperature is raised.

(c) What is the effect of a finite T_2 on $\gamma(\omega)$?

15.6 Consider the effect on the modulation response $p_1(\omega_m)/i_1(\omega_m)$ of the inclusion of a nonlinear gain term bP in the rate equations (15.6-1)

$$\frac{dN}{dt} = \frac{I}{eV} - \frac{N}{\tau} - A(1 - bP)(N - N_{\text{tr}})P$$
$$\frac{dP}{dt} = A(1 - bP)N - N_{\text{tr}})P\Gamma_a - \frac{P}{\tau_p}$$

where $bP \ll 1$. Show that the main effect is a damping of the resonance peak at ω_R.

15.7 Solve for the carrier density modulation $N = N_0 + N_1\, e^{i\omega_m t}$ in a semiconductor laser whose current is modulated at

$$I = I_0 + I_1 e^{i\omega_m t} \tag{1}$$

$$\omega_m = \text{modulation frequency} \ll \omega_{\text{opt}} \tag{2}$$

(See Section 15.6.)

15.8 Assume $\epsilon = \epsilon_0 - aN$, a is a constant and that the instantaneous frequency of the semiconductor laser obeys

$$\frac{\Delta\nu}{\nu} = -\frac{\Delta\epsilon}{\epsilon} \tag{3}$$

find the form of the laser optical field due to the current modulation. What is the (phase) modulating index of the field?

15.9 Using the data of Figure 15-7, what is the total current needed to render the active medium of a semiconductor laser transparent? Assume an active volume of $300 \times 2 \times 0.2$ (μm^3) and a recombination lifetime of $\tau = 3 \times 10^{-9}$ seconds.

15.10 If the thickness of the active region in Problem 15.9 were reduced to

100 Å, can we obtain enough gain from a semiconductor laser to overcome a distributed loss constant of $\alpha = 20\ \text{cm}^{-1}$ and $R = 0.9$? What will be the transparency current? What will be the threshold current? Assume a mode height normal to the interfaces of $t = 4000$ A and

$$\Gamma_a \sim \frac{\text{d(active region)}}{\text{t(mode height)}}$$

References

1. Basov, N. G., O. N. Krokhin, and Y. M. Popov, "Production of negative temperature states in *p-n* junctions of degenerate semiconductors," *J.E.T.P.* 40:1320, 1961.
2. Hall, R. N., G. E. Fenner, J. D. Kingsley, T. J. Soltys, and R. O. Carlson, "Coherent light emission from GaAs junctions," *Phys. Rev. Lett.* 9:366, 1962.
3. Nathan, M. I., W. P. Dumke, G. Burns, F. H. Dills, and G. Lasher, "Stimulated emission of radiation from GaAs *p-n* junctions," *Appl. Phys. Lett.* 1:62, 1962.
4. Yariv, A., and R. C. C. Leite, "Dielectric waveguide mode of light propagation in *p-n* junctions," *Appl. Phys. Lett.* 2:55, 1963.
5. Anderson, W. W., "Mode confinement in junction lasers," *IEEE J. Quant. Elec.* QE-1:228, 1965.
6. Kittel, C., *Introduction to Solid State Physics,* 5th ed. New York: Wiley, 1982.
7. Yariv, A., *Introduction to the Theory and Applications of Quantum Mechanics.* New York: Wiley, 1982.
8. Bernard, M. G., and G. Duraffourg, "Laser conditions in semiconductors," *Phys. Status Solidi* 1:699, 1961.
9. Vahala, K., L. C. Chiu, S. Margalit, and A. Yariv, "On the linewidth enhancement factor α in semiconductor injection lasers," *Appl. Phys. Lett.* 42:631, 1983.
10. Stern, F., "Semiconductor lasers: Theory," *Laser Handbook,* F. T. Arecchi and E. O. Schultz Du Bois, eds. Amsterdam: North Holland, 1972.
11. Kressel, H., and J. K. Butler, *Semiconductor Lasers and Heterojunction LEDS.* New York: Academic Press, 1977.
12. Yariv, A., *Quantum Electronics,* 2d ed. New York: Wiley, 1975, p. 219.
13. Casey, H. C., and M. B. Panish, *Heterostructure Lasers.* New York: Academic Press, 1978.
14. Dupuis, R. D., and P. D. Dapkus, *Appl. Phys. Lett.* 31:466, 1977.
15. Cho, A. Y., and J. R. Arthur, in *Progress in Solid State Physics,* J. O. McCaldin and G. Somoraj, eds., vol. 10. Pergamon Press, p. 157.
16. Tsang, W. T. and A. Y. Cho, "Growth of GaAs/GaAlAs by molecular beam epitoxy," *Appl. Phys. Lett.* 30:293, 1977.

17. Hayashi, J., M. B. Panish, and P. W. Foy, "A low-threshold room-temperature injection laser," *IEEE J. Quant. Elec.* 5:211, 1969.
18. Kressel, H., and H. Nelson, "Close confinement gallium arsenide *p-n* junction laser with reduced optical loss at room temperature," *RCA Rev.* 30:106, 1969.
19. Alferov, Zh. I., et al., *Sov. Phys.—Semicond.*, 4:1573, 1971.
20. Tsukada, T., "GaAs-$Ga_{1-x}Al_xAs$ buried heterostructure injection lasers," *J. Appl. Phys.* 45:4899, 1974.
21. Chinone, N., H. Nakashima, I. Ikushima, and R. Ito, "Semiconductor lasers with a thin active layer (<0.1 μm) for optical communication," *Appl. Opt.* 17:311, 1978.
22. Botez, D., and G. J. Herskowitz, "Components for optical communication systems: A review," *Proc. IEEE* 68: 1980.
23. Ortel Corp., Alhambra, Calif. Product Data Sheets.
24. Hsieh, J. J., J. A. Rossi, and J. P. Donnelly, "Room temperature CW operation of GaInAsP/InP double heterostructure diode lasers emitting at 1.1 μm," *Appl. Phys. Lett.* 28:709, 1976.
25. Yu, K. L., Koren, U., T. R. Chen, and A. Yariv, "A Groove GaInAsP Laser on Semi-Insulating InP," *IEEE J. Quant. Elec.* QE-8:817, 1982.
26. Suematsu, Y., "Long wavelength optical fiber communication," *Proc. IEEE.* 71:692, 1983.
27. Lau, K. T., N. Bar-Chaim, I. Ury, and A. Yariv, "Direct amplitude modulation of semiconductor GaAs lasers up to X-band frequencies," *Appl. Phys. Lett.* 43:11, 1983.
28. Lau, K. Y., Ch. Harder, and A. Yariv, "Direct modulation of semiconductor lasers at $f > 10$ GHz," *Appl. Phys. Lett.* 44:273–275, 1984.
29. See, for example, Bailbe, J. P., A. Marty, P. H. Hiep, and G. E. Rey, "Design and fabrication of high speed GaAlAs/GaAs heterojunction transistors," *IEEE Trans. Elect. Dev.* ED-27:1160, 1980.
30. Yariv, A., "Active integrated optics," in *Fundamental and Applied Laser Physics,* Proc. ESFAHAN Symposium, Aug. 29, 1971, M. S. Feld, A. Javan, N. Kurnit, eds. New York: Wiley, 1972.
31. Ury, I., K. Y. Lau, N. Bar-Chaim, and A. Yariv, "Very high frequency GaAlAs laser-field effect transistor monolithic integrated circuit," *Appl. Phys. Lett.* 41:126, 1982.
32. Yust, M., et al., "A monolithically integrated optical repeater," *Appl. Phys. Lett.* 10:795, 1979.
33. Bar-Chaim, N., I. Ury, and A. Yariv, "Integrated optoelectronics," *IEEE Spectrum,* p. 38, May 1982.
34. Hernandez-Gil, F., T. L. Koch, U. Koren, R. P. Gnall, C. A. Burrus, "Tunable MQW-DBR laser with a monolithically integrated InGaAsP/InP Directional coupler switch," paper PD 17, Conference on Laser Engineering and Optics (CLEO) 1989.
35. Koren, U., et al., "Wavelength division multiplexing light source with

integrated quantum well tunable lasers and optical amplifiers," *Appl. Phys. Lett.* 54:21 (May 1989).

36. Harder, C., K. Vahala, and A. Yariv, "Measurement of the linewidth enhancement factor α of semiconductor lasers," *Appl. Phys. Lett.* 42:428 (1983).

37. Koch, T., and J. Bowers, "Nature of wavelength chirping in directly modulated semiconductor lasers," *Electr. Lett.* 20:1038–1040, 1984.

38. Derry, P., et al., "Ultra low threshold graded-index separate confinement single quantum well buried heterostructure (Al, Ga) as lasers with high reflectivity coatings," *Appl. Phys. Lett.* 50:1773, 1987.